Available online at www.sciencedirect.com
SCIENCE DIRECT®
Physica D 189 (2004) 70–80
PHYSICA D
www.elsevier.com/locate/physd

Global manifold control in a driven laser: sustaining chaos and regular dynamics

R. Meucci [a], D. Cinotti [a], E. Allaria [a,*], L. Billings [b], I. Triandaf [c], D. Morgan [c], I.B. Schwartz [c]

[a] *Istituto Nazionale di Ottica Applicata, Largo E. Fermi 6, 50125 Firenze, Italy*
[b] *Department of Mathematical Sciences, Montclair State University, Upper Montclair, NJ 07043, USA*
[c] *Naval Research Laboratory, Plasma Physics Division, Code 6792, Washington, DC 20375-5000, USA*

Received 27 June 2003; received in revised form 8 September 2003; accepted 26 September 2003
Communicated by R. Roy

Abstract

We present experimental and numerical evidence of a multi-frequency phase control able to preserve periodic behavior within a chaotic window as well as to re-excite chaotic behavior when it is destroyed by the presence of a mitigating unstable periodic orbit created in the presence of the multi-frequency drive. The mitigating saddle controlling the global behavior is identified and the controlling manifolds approximated.

Keywords: Driven laser; Chaos dynamics; Regular dynamics

1. Introduction

Control of chaos represents one of the most interesting and stimulating ideas in the field of nonlinear dynamics [1]. The original basic idea is to stabilize the dynamics over one of the different unstable periodic orbits visited during the chaotic motion by applying small perturbations to the system [2]. Alternatively, one may wish to sustain chaos in certain situations where chaos is destroyed [3,4]. Both stabilizing unstable orbits and sustaining chaos by exciting unstable chaotic orbits may be considered as intervention techniques to control the dynamical flow.

Different methods for controlling chaos have been proposed based on determination of the stable and unstable manifolds on the Poincaré section [2,5–7], on a self-controlling feedback procedure [8] and on the introduction of open loop small perturbations [9–16].

On the other hand, chaos can be a desirable behavior in biological [4], mechanical [17], electrical [18] and optical systems [19]. In mechanics, small amplitude chaos, where the energy is spread over several modes, may be preferable to high amplitude resonant behavior [20,21]. In such situations, the chaotic attracting window may be quite small, and sustained chaos techniques are therefore required.

Once a chaotic regime appears, it typically and dramatically disappears as a result of a crisis, which is an abrupt change from chaos to periodic behavior at a critical parameter value of the system [22]. The

* Corresponding author. Tel.: +39-055-23081; fax: +39-055-2337755.
E-mail addresses: ric@ino.it (R. Meucci), allaria@ino.it (E. Allaria).

0167-2789/$ – see front matter © 2003 Elsevier B.V. All rights reserved.
doi:10.1016/j.physd.2003.09.033

crisis typically occurs when the chaotic attractor collides with the stable manifold of an unstable periodic orbit, this stable manifold being, at the same time, the basin boundary of the chaotic attractor [23,24]. Such a saddle is called a basin saddle since it lies on the basin boundary of the attractor and regions around such a saddle form escape regions for the chaotic trajectories resulting in non-chaotic behavior. Previous techniques for sustaining chaos have been designed around a feedback control mechanism in which a parameter or state variable was used to maintain chaos by re-injecting the dynamics into a region containing a chaotic saddle from a basin containing periodic attractors [4,17,18,25–27]. In contrast, the global topology of the basin boundary saddle manifold structure may be used to design parameter control algorithms for sustaining chaos in parameter regimes where a crisis occurs [3,28]. Chaos is sustained by adjusting a system parameter discretely based on measuring a time series obtained from the system, and using embedding methods to reconstruct the dynamics in a phase space [3].

Closed loop control techniques have been demonstrated in fast electronic oscillators and in principle applicable in optical systems with latency time below 1 ns [29]. However for controlling and sustaining chaos in systems such as those having fast time scales open loop methods are desirable for two primary reasons: (1) Open loop control methods have no feedback time scale with which to compete. (2) Many nonlinear optical systems now are sufficiently modeled so that there exists excellent quantitative agreement between theory and experiment.

In the present paper we take an open loop approach to control and sustaining chaos. Let us first consider the latter aspect. The approach still excites chaos, but it is an open-loop procedure that can be designed so that stable chaotic regions may be achieved in places where these were not stable previously. The procedure starts with a periodically driven system at a primary frequency having a drive amplitude as an adjustable parameter. The drive amplitude is tuned so that the system operates in a crisis regime. Introduction of additional subharmonics may be expected to change local bifurcations, as well as global bifurcations. It is well known that additive subharmonic perturbations shift period doubling points in a cascade to chaos [30]. However, it may also change the nature of the bifurcation, where flip bifurcations become imperfect bifurcations containing multiple stability and new saddle-node points. Since the manifolds controlling the global behavior are typically connected to regular saddles arising from such limit point bifurcations, it is expected that global bifurcations such as crises will be changed when introducing resonant subharmonics.

The adopted strategy in our modulated laser is to consider an amplitude modulation at half of the driving frequency. We notice that the used perturbation is equivalent to applying an additive perturbation with components at $\nu/2$ and $3\nu/2$. In addition, a phase difference between the amplitude modulation and primary frequency is considered as an extra parameter. The relevance of such a parameter in the framework of control of chaos has been demonstrated in experimental [13,16,31,32] and numerical works [14]. The addition of the amplitude modulation allows global manifold control at low energies in fast time scale systems. Moreover, it is easily implemented in a large class of experiments that are forced by an external drive frequency.

The advantage of our method is that we can initiate regular (controlled) periodic behavior or sustained chaos without any knowledge of a crisis in a chaotic attractor.

2. Experimental apparatus and measurements

The experimental apparatus is shown in Fig. 1. It consists in a single mode CO_2 laser with an intra-cavity acousto-optic modulator (AOM) allowing modulation of the cavity losses. The optical cavity is 1.30 m long and the total transmission coefficient T is 0.10 for a single pass. The intensity decay rate $k(t)$ can be expressed as follows:

$$k(t) = k[1 + \alpha \sin^2(B_0(1 + f(t)))], \quad (1)$$

where $k = cT/L$, c is the speed of light in a vacuum, L the cavity length, $\alpha = (1 - 2T)/2T$, B_0 is a bias

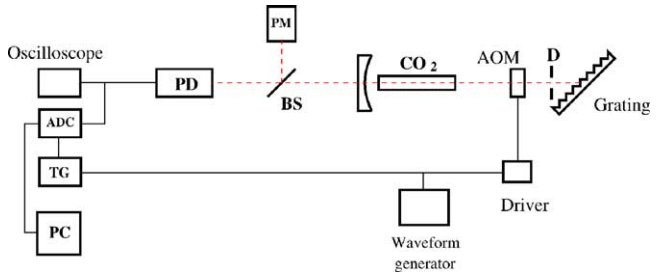

Fig. 1. Experimental apparatus used to perform our measurements. AOM: acousto-optic modulator; BS: beam splitter; PM: power meter; PD: photodetector; TG: trigger generator; ADC: analog to digital converter; PC: personal computer.

and $f(t)$ is the modulation signal,

$$f_{\mathrm{mod}}(t) = \beta \sin(2\pi\nu t), \tag{2}$$

where $\nu = 100\,\mathrm{kHz}$ and β is the modulation amplitude. It is well known that by increasing the amplitude modulation, the system undergoes a sequence of subharmonic bifurcation leading to chaos. A programmable arbitrary function generator (FG) allow us to linearly scan the whole range of β by generating the function (2) where β is a saw tooth which goes from 0 to 1 V in 200 ms. In this configuration we do not consider hysteresis effects related to the scan in the opposite direction.

In Fig. 2 the bifurcation diagram is shown, where we plot a stroboscopic record of the intensity versus the amplitude modulation. The sampling period is $1/\nu$ and the scanning time is 200 ms. From the bifurcation diagram we observe the presence of a first chaotic region ("chaos 1") reached after a sequence of subharmonic bifurcations. When the control parameter β is increased up to $\beta \simeq 570\,\mathrm{mV}$ we observe the presence of an *interior crisis* leading to a sudden expansion of the attractor. We denote such a region as "chaos 2". The "chaos 2" window is sudden destroyed by a *boundary crisis* at $\beta \simeq 900\,\mathrm{mV}$.

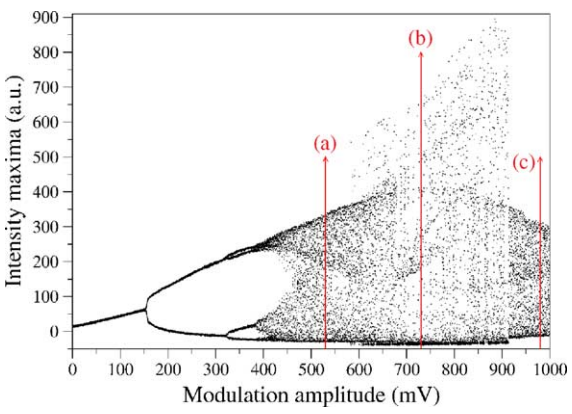

Fig. 2. Experimental bifurcation diagram of the laser intensity as a function of the amplitude modulation β. The first chaotic window is reached through a sequence of subharmonic bifurcations occurring at $\beta \simeq 150\,\mathrm{mV}$, the second one at $\beta \simeq 320\,\mathrm{mV}$. We note the interior crisis at $\beta \simeq 570\,\mathrm{mV}$.

Control and sustaining chaos are obtained by slight modulation of the modulation amplitude β. Such a perturbation consists of a sinusoidal signal at $\nu/2$ with amplitude δ and an adjustable phase offset φ with respect to the fundamental signal $f_{\mathrm{mod}}(t)$; then the modulation signal becomes:

$$f_{\mathrm{mod}}(t) = \beta[1 + f_{\mathrm{pert}}(t)] \sin(2\pi\nu t),$$
$$f_{\mathrm{pert}}(t) = \delta \sin\left(2\pi\frac{\nu}{2}t + \varphi\right). \tag{3}$$

The advantage of the subharmonic control approach is that it is easy to implement in many time forced experiments, regardless of time scales.

In Fig. 3, we report the perturbed bifurcation diagram as a function of β for three different values of φ and for a fixed perturbation amplitude δ of 5%. Around $\beta = 500\,\mathrm{mV}$, the perturbation stabilizes the period-2 orbit visited in the "chaos 1" regime. We note that this control effect is greater for $\varphi = \pi/2$. We also note a sustaining chaos effect at the end of the bifurcation diagram, where region "chaos 2" was destroyed by a boundary crisis. The applied perturbation is able to re-excite this attractor, with the result that small parameter perturbations at 1/2 the drive frequency have a global effect.

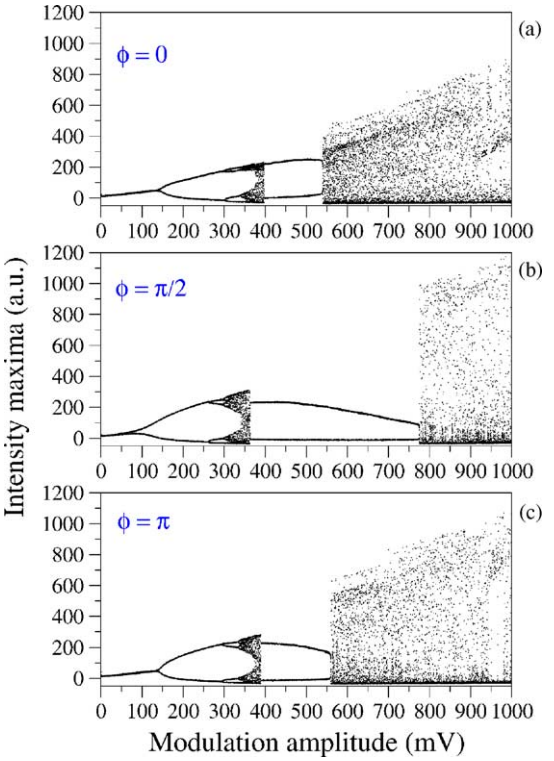

Fig. 3. Experimental perturbed bifurcation diagrams of the intensity laser as a function of modulation amplitude β for different values of the phase φ. We can see the controlled periodic orbit for β around 500 mV and the sustained chaos at the end of the bifurcation diagrams.

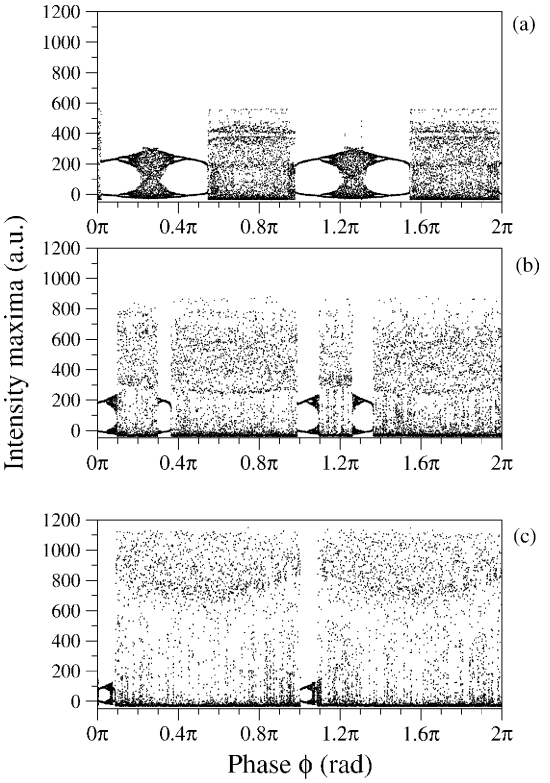

Fig. 4. Experimental phase control diagrams of the intensity laser as a function of the phase φ. Modulation amplitude is chosen: (a) in the first "chaos 1" window; (b) in "chaos 2" window; (c) in the second "chaos 2" window (compare with Fig. 2). The relevance of the phase term to sustain or control chaos is evident. The origin of the horizontal axis (phase) is arbitrary because the trigger is not locked with the origin of the saw tooth.

In Fig. 4, we report stroboscopic recordings of the intensity as a function of the phase at a fixed value of amplitude modulation β. These phase control diagrams refer to three amplitude values β corresponding to the first "chaos 1" window ($\beta = 530$ mV), to the "chaos 2" window ($\beta = 730$ mV) and to the second "chaos 1" window ($\beta = 940$ mV), respectively. We note that there are some φ values for which we have chaos control ($\beta = 530$ mV, $\varphi \in [0, 0.15\pi]$ and $[0.4\pi, 0.55\pi]$, $\beta = 730$ mV, $\varphi \in [0, 0.05]$ and $[0.3\pi, 0.35\pi]$, $\beta = 940$ mV, $\varphi \in [0, 0.05\pi]$) and other for which we have sustaining chaos ($\beta = 530$ mV, $\varphi \in [0.55\pi, 0.95\pi]$, $\beta = 940$ mV, $\varphi \in [0.1\pi, \pi]$). Fig. 4a shows that, although the period-2 regime is the most easier to stabilize, there are values for the phase φ where period-4 orbit is also stabilized.

Although not all orbits embedded in the chaotic attractor are stabilized, we can, in principle, stabilize other periods by adding other subharmonics. However, for the purposes of control presented here, the goal is to be able to sustain chaos or stabilize regular periodic behavior.

Notice that as the modulation amplitude changes, so does the region over which chaos is excited. Since the phase changes the observed behavior between regular and chaotic behavior for each chosen amplitude, it plays a prominent role in determining control or sustained chaos.

In Fig. 5, we compare the unperturbed "chaos 2" Poincaré section (Fig. 5a) with one perturbed (Fig. 5b). Similarity between the projected phase space portraits suggests that our method re-excites the chaotic saddle corresponding to the original pre-crisis saddle.

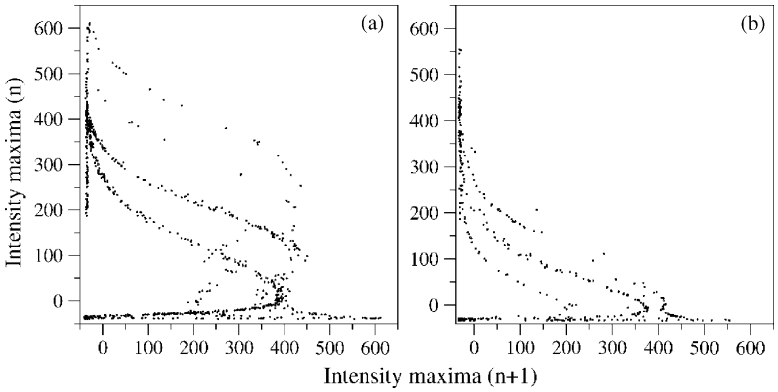

Fig. 5. Poincaré sections of the "chaos 2" regime: (a) in the unperturbed case $\beta = 730\,\text{mV}$; (b) in the perturbed case with $\beta = 530\,\text{mV}$ and $\varphi = 0.8\pi$. The similarities between the two sections *suggests* that we are exciting the same chaotic attractor.

3. Numerical analysis on a CO_2 laser model

The model we use in our simulations is a four-level model (4LM) which consists of five differential equations for the intensity I, the populations of the upper and lower lasing states N_2 and N_1, and the global populations M_2 and M_1 of the two manifolds of rotational levels which are coupled by collisions with N_2 and N_1, respectively:

$$\begin{aligned}
\dot{I} &= -k(t)I + G(N_2 - N_1)I,\\
\dot{N}_2 &= -(z\gamma_R+\gamma_2)N_2 - G(N_2-N_1)I + \gamma_R M_2+\gamma_2 P,\\
\dot{N}_1 &= -(z\gamma_R + \gamma_1)N_1 + G(N_2 - N_1)I + \gamma_R M_1,\\
\dot{M}_2 &= -(\gamma_R + \gamma_2)M_2 + z\gamma_R N_2 + z\gamma_2 P,\\
\dot{M}_1 &= -(\gamma_R + \gamma_1)M_1 + z\gamma_R N_1,
\end{aligned} \tag{4}$$

where $\gamma_R = 7.0 \times 10^5\,\text{Hz}$ is the relaxation rate between the lasing states and the associated rotational manifolds (the enhancement factor $z = 10$ represents the number of sublevels considered in each manifold), and $\gamma_2 = 1.0 \times 10^4\,\text{Hz}$ and $\gamma_1 = 8.0 \times 10^4\,\text{Hz}$ are the relaxation rates of the vibrational states. Moreover, $G = 6.2 \times 10^{-8}\,\text{Hz}$ is the field–matter coupling constant, while the non-dimensional parameter $P = 5.16 \times 10^{14}$ represents the pump. We have re-scaled the model by introducing new non-dimensional variables:

Table 1

$x_1 = \dfrac{G}{k} \cdot I$	$k_0 = \dfrac{k}{\gamma_R} = 32.97$
$x_2 = \dfrac{G}{k} \cdot (N_2 - N_1)$	$\Gamma_1 = \dfrac{\gamma_1 + \gamma_2 + 2z\gamma_R}{2\gamma_R} = 10.0643$
$x_3 = \dfrac{G}{k} \cdot (N_2 + N_1)$	$\Gamma_2 = \dfrac{\gamma_1 + \gamma_2 + 2\gamma_R}{2\gamma_R} = 1.0643$
$x_4 = \dfrac{G}{k} \cdot (M_2 - M_1)$	$\gamma = \dfrac{\gamma_1 - \gamma_2}{2\gamma_R} = 0.05$
$x_5 = \dfrac{G}{k} \cdot (M_2 + M_1)$	$P_6 = \dfrac{\gamma_2 PG}{k\gamma_R} = 0.016$
$\alpha = 4$	$k_1(\tau) = \dfrac{k(t)}{\gamma_R} = k_0[1 + \alpha\,\sin^2(B_0(1 + f(t)))]$
$B_0 = 0.2$	$f(t) = \beta \sin(\omega\tau)$
$\beta = [0, 1]$	$\omega = \dfrac{2\pi\nu}{\gamma_R} = 0.89759$

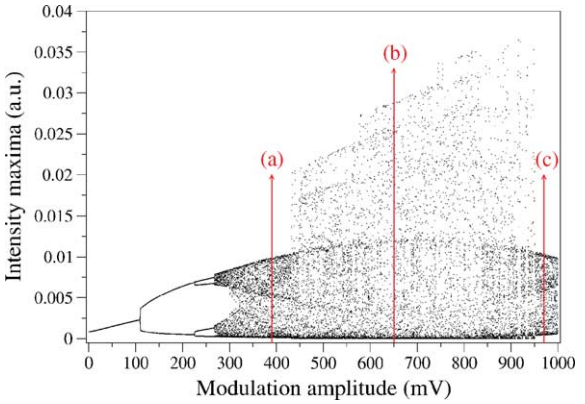

Fig. 6. Numerical bifurcation diagram of the intensity laser form Eq. (3) as a function of the modulation amplitude β.

$$
\begin{aligned}
\dot{x}_1 &= -k_1(\tau)x_1 + k_0 x_1 x_2,\\
\dot{x}_2 &= -\Gamma_1 x_2 - 2k_0 x_1 x_2 + \gamma x_3 + x_4 + P_6,\\
\dot{x}_3 &= -\Gamma_1 x_3 + \gamma x_2 + x_5 + P_6,\\
\dot{x}_4 &= -\Gamma_2 x_4 + z x_2 + \gamma x_5 + z P_6,\\
\dot{x}_5 &= -\Gamma_2 x_5 + z x_3 + \gamma x_4 + z P_6,
\end{aligned}
\tag{5}
$$

where $\tau = \gamma_R \cdot t$ is the re-scaled time and new variables and constants are given in Table 1.

Using this re-scaled model we reproduce the experimental bifurcation measurements with a good degree of accuracy. We have performed simulations modulating the losses with a signal according with Eq. (3) assuming a bias value $B_0 = 0.2$. The agreement of the model with the experiment can be inferred from Fig. 6, showing the unperturbed bifurcation diagram, and from Fig. 7 where we report three perturbed

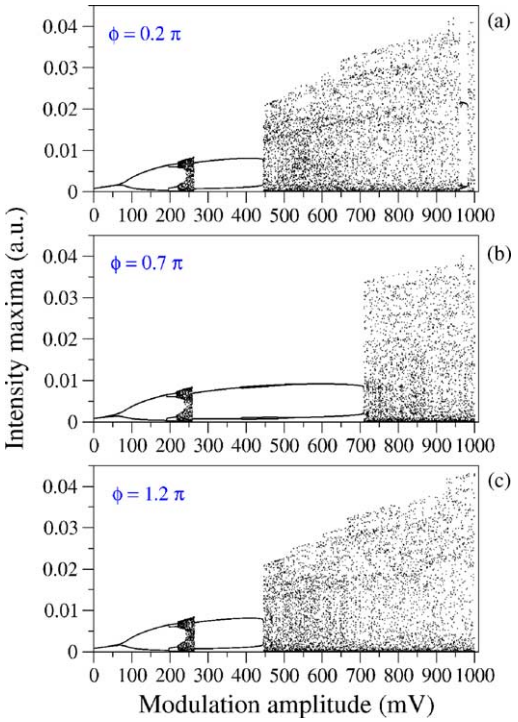

Fig. 7. Numerical perturbed bifurcation diagrams of the laser intensity as a function of amplitude modulation β. (a) $\varphi = 0.2$; (b) $\varphi = 0.7\pi$; (c) $\varphi = 1.2\pi$. The correspondence with the experimental results shown in Fig. 3 is clear. We note that there is a slight phase shift between experiment and numerical analysis.

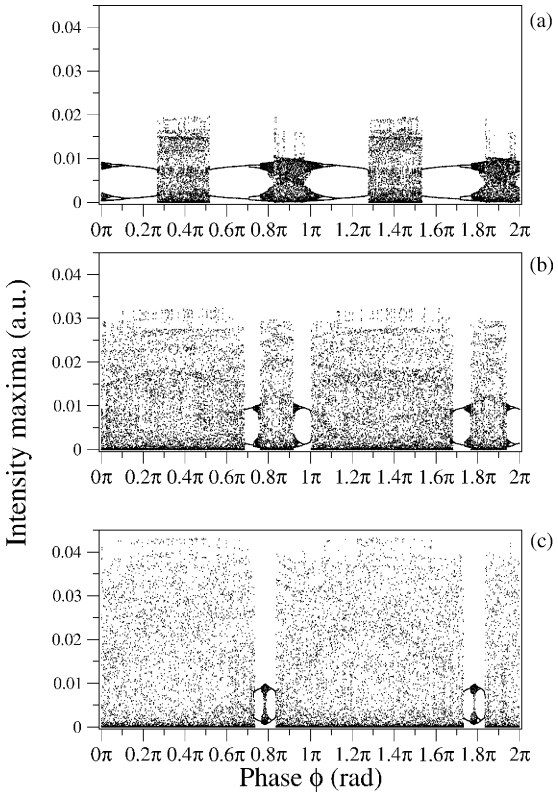

Fig. 8. Numerical perturbed bifurcation diagrams of the intensity laser as a function of the phase φ. Modulation amplitude is chosen: (a) in the first "chaos 1" window; (b) in "chaos 2" window; (c) in the second "chaos 2" window as in the experiment (compare with Fig. 6).

bifurcation diagrams. In Fig. 8, we report other numerical results corresponding to the experimental measurements shown in Fig. 1. The comparisons show that the agreement between theory and experiment is excellent. Moreover, since the bifurcation diagrams agree on large parameter scales, the agreement is global.

4. Manifold control in the subharmonic laser

The reconstruction of the topology of the basin boundary saddle manifold structure is more easily performed by using a suitable reduction of the five-dimensional model of Eq. (5). We perform such a reduction by approximating to the same value $((\gamma_1 + \gamma_2)/2)$ the two relaxation rates γ_1 and γ_2 in Eq. (4). This implies in Eq. (5) $\gamma = 0$ and the same values for Γ_1 and Γ_2.

The relevant variables are x_1, the population level difference, x_2, and the rotational level difference, x_4. In this reduction procedure, a crucial role is played by the pump parameter P_{inf} which has been readjusted in order to provide the same steady state value of the laser intensity x_1. The main features of the full model are retained by the following reduced 3D model:

$$\begin{aligned}
\dot{y}_1 &= k_0(y_2 - 1 - \alpha \sin^2(f_{\text{mod}} + B_0)),\\
\dot{y}_2 &= -\Gamma_1 y_2 - 2k_0\, e^{y_1} y_2 + y_3 + P_{\text{inf}},\\
\dot{y}_3 &= -\Gamma_2 y_3 + z y_2 + z P_{\text{inf}},\\
f_{\text{mod}} &= A_{\text{mod}}(1 + f_{\text{pert}}) \sin(\omega t),\\
f_{\text{pert}} &= A_{\text{pert}} \sin\left(\frac{\omega t}{2} + \phi\right)
\end{aligned} \tag{6}$$

with the parameter $P_{\text{inf}} = 0.0815$. Notice the similarity of the bifurcation diagram in Fig. 9 to that of Fig. 2 from the experiment and Fig. 6 and the model.

By using the subharmonic amplitude modulation it is possible to control the chaotic behavior by acting on the relative phase ϕ [33]. As an example, we compute the maximal Lyapunov exponent for $A_{\text{mod}} = 0.1$ as a function of subharmonic amplitude A_{pert} and phase ϕ to show the effect of the applied perturbation. The results are depicted in Fig. 10.

For $A_{\text{pert}} = 0.05$, Fig. 11 shows the bifurcation diagram as a function of the phase ϕ in phase space.

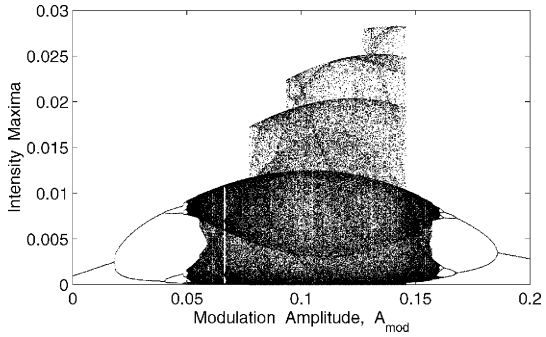

Fig. 9. Bifurcation diagram of the intensity as a function of modulation amplitude, A_{mod} using Eq. (6). No subharmonic forcing was applied.

Notice the four windows where large amplitude chaos changes to a low-order stable periodic orbit. Fig. 10 also predicts this change by an absence of a positive Lyapunov exponent. The generic crisis bifurcation from chaos to periodic behavior is caused by the creation of a saddle-node pair of periodic orbits of period one when time is normalized to $4\pi/\omega$. (There also exists a very small, four-piece chaotic attractor, which is long lived for these parameters that is not observed in the experiment and does not seem to play a significant role in the dynamics.) There are two transient time scales in the convergence to the periodic attractor. The first is convergence from the immediate basin, which

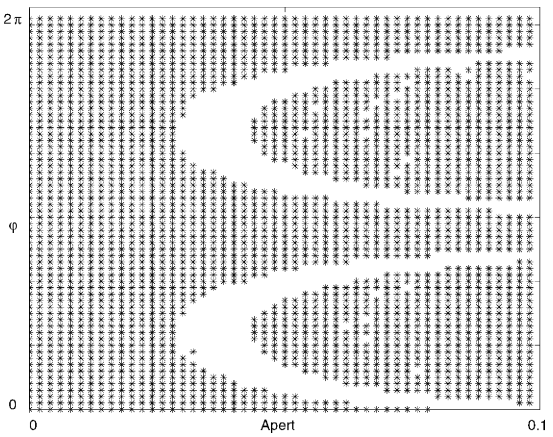

Fig. 10. Maximal Lyapunov exponent of the 3D model as a function of the subharmonic modulation amplitude, A_{pert} and phase, ϕ using Eq. (6) with $A_{\text{mod}} = 0.1$. Asterisks denote parameters which generate a positive exponent for some random initial condition.

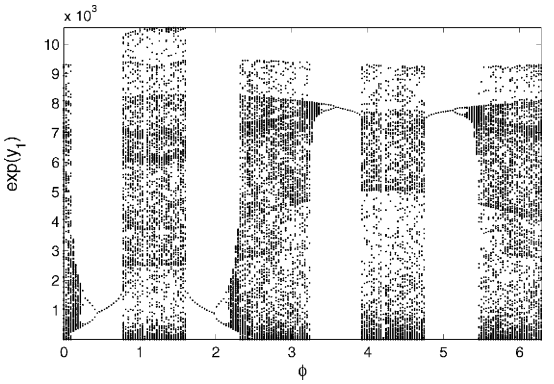

Fig. 11. Control phase diagrams for $A_{\text{mod}} = 0.1$ and $A_{\text{pert}} = 0.05$.

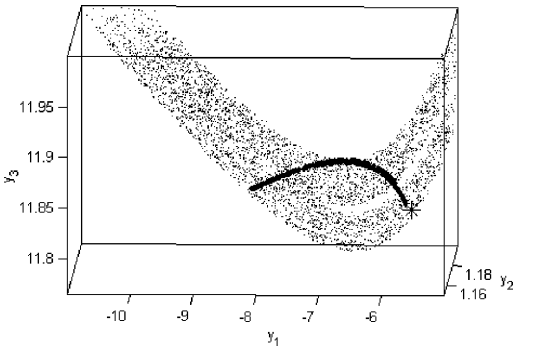

Fig. 12. Small amplitude chaotic attractor in large black dots just before the bifurcation to a large amplitude attractor. The star represents the period one saddle and the small black dots represent its stable manifold. The parameters are $A_{\text{mod}} = 0.1$, $A_{\text{pert}} = 0.05$, and $\phi = 2.28$.

is bounded by the two-dimensional stable manifold of the associated period one saddle. The other is a slower convergence after a significant chaotic transient, along the chaotic saddle left by the chaotic attractor from before the bifurcation.

Notice that in the interval $1.6 < \phi < 2.3$, after the bifurcation from large amplitude chaos to a stable period one orbit, the stable periodic orbit goes through a period doubling cascade to small amplitude chaotic dynamics. At the end of the window, there is another bifurcation back to large amplitude chaos. This bifurcation is caused by a crisis, when the small amplitude chaotic attractor intersects the stable manifold of the period one saddle from the original saddle node bifurcation that created the window. The two-dimensional version of this bifurcation was reported in [33]. In Fig. 12, we plot the relevant period one saddle at $(y_1, y_2, y_3) = (-5.5657, 1.1588, 11.8413)$ and its stable manifolds for $\phi = 2.28$, just prior to the onset of the large amplitude chaotic attractor. It is the outer shell of the union of the stable manifolds, represented by the small black points which lie on two-dimensional folded sheets. Overlaid in large black points is a sample small amplitude chaotic trajectory. This set is embedded in one of the unstable manifolds of the saddle. As ϕ increases, the chaotic set intersects the stable manifold of the period one saddle, similar to a homoclinic bifurcation since *the attractor is contained in the unstable manifold*, and a crisis to large amplitude chaos occurs. That is, since the attractor is a subset of the unstable manifold, the attractor itself explodes in phase space upon intersection with the stable manifold sheet, creating the large amplitude attractor.

The stable and unstable manifolds in the phase space can be approximated by the box-algorithm described in [34]. Briefly, the algorithm works as follows: Pick a region of interest interior to a box, B, containing the unstable saddle with part of its stable and unstable manifolds. (If the box also contains periodic points which are attractors, then we put a small neighborhood about these points, and the box is a punctured set.) Inside that box we randomly pick a large number of initial conditions and record which of these initial conditions will generate trajectories remaining in the box for a large number of iterations. In addition we monitor a small neighborhood of any attracting orbits contained in B, and eliminate any points converging to this attractor, since these points will not represent the manifolds we approximate. The initial conditions remaining in the punctured box approximate the union of the stable manifolds, while the last point which remains in the box approximates the unstable manifolds. This algorithm was used to generate the stable manifolds in Fig. 12.

In summary for the example of $A_{\text{mod}} = 0.1$ and $A_{\text{pert}} = 0.05$, when there exists a periodic attractor, it is connected to a minimal period one branch. These attracting branches are born through a saddle node pair, typically embedded in a large amplitude chaotic attractor for some ϕ. It is the manifold of the saddle

branches which destroys and creates the regions of large amplitude chaos, and therefore, acts as the controlling mechanism for the sustaining of chaos in a region in which the primary frequency has only periodic behavior.

5. Conclusions

We have presented an open-loop control procedure to induce and control chaos in periodically driven systems. The method is based on driving the system with a 1:2 resonance modulation and varying the amplitude and the phase of the drive in this modulation. Open-loop control can either sustain chaos or stabilize regular periodic orbits, and is achieved through global manifold control through the creation of a saddle-node bifurcation.

We have applied the procedure to a periodically driven CO_2 laser and we have experimentally sustained or controlled chaos depending on the value of the relative phase between perturbation and modulation. Based on the choice of control parameters, the regions over which either regular periodic behavior or chaos may be sustained can be quite large, as seen in Fig. 10.

In order to verify our experimental measurements, we applied the method to a well tested 5-equation CO_2 laser model; the numerical results match the experimental results with good agreement. We have reduced this model to a lower dimensional model in order to visualize the manifolds which are connected to an unstable periodic saddle created by the subharmonic term.

We would like to acknowledge the fact that although there exist a number of papers on multi-frequency driving and bifurcation, most of them are driven planar models, and those that have any global bifurcation results are based on a Melnikov method, which is useful in mechanics. In our results, we have considered a model which has been reduced to a three-dimensional multi-frequency system, and captures much of the experimentally observed dynamics over a wide range of parameters. The primary controlling mechanism is the interaction of a two-dimensional stable manifold with a one-dimensional unstable manifold. The stable manifold consists of two-dimensional sheets which possess a fractal-like structure. As the control parameters are adjusted, the stable and unstable manifolds cross and uncross transversally, yielding the sustained chaos or regular periodic behavior which is observed in both numerical and experimental dynamics. One of the interesting facets of the use of multi-frequency control is that it may also be applied to discrete systems as well as continuous flows. In Appendix A we have shown that one may drive a map in much the same way as we have done in the experiment. Specifically, we have applied our procedure to the logistic map; we established chaos control in some range of φ value and sustaining chaos in some other one. Because the sustaining chaos and control procedure is effective also in this case, we can affirm its generality to both continuous and discrete dynamical systems.

Acknowledgements

RM and EA are supported by the European Contract HPRN CT 2000 00158. IBS and IT are supported by the Office of Naval Research. LB was supported by ONR grant N00173-02-G909. DM is a National Research Council Post Doctoral Fellow. We would like to acknowledge Prof. Thomas Carr for useful discussions, and for pointing out some of analytic local bifurcation results in the literature.

Appendix A. Sustaining chaos in the logistic map

The logistic map is described by the difference equation:

$$x_{n+1} = Ax_n(1 - x_n), \tag{A.1}$$

where $x_n \in [0, 1]$ if $A \in (0, 4)$. The Lyapunov exponent λ of the map, can be evaluated as follows:

$$\lambda = \lim_{n\to\infty} \frac{1}{n} \sum_{i=0}^{n-1} \ln |A(1 - 2x_i)|, \tag{A.2}$$

where in our calculation $n = 1500$.

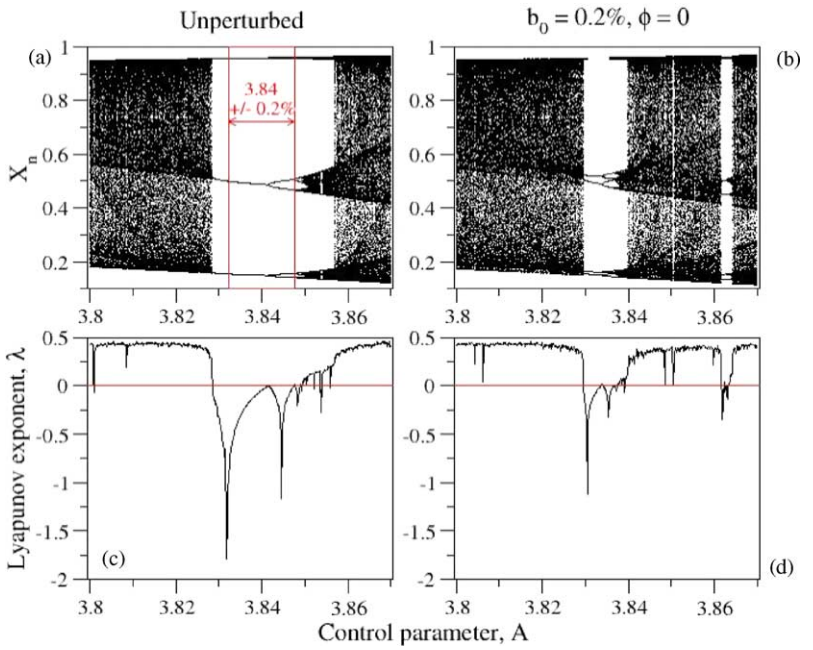

Fig. 13. Bifurcation diagrams for the logistic map for $A \in [3.8, 3.87]$. Left: unperturbed; right: $b_0 = 0.002$, $\varphi = 0$. In the perturbed case we note the partial destruction of the periodic window around $A = 3.84$ (sustaining chaos) and the new periodic window near $A = 3.86$.

We extend our chaos sustaining procedure to Eq. (A.1) as follow:

$$A = A_0 \left[1 + b_0 \cos\left(2\pi\left(\frac{n}{2} + \varphi\right)\right)\right], \qquad \text{(A.3)}$$

where $b_0 = 0.002$ is the perturbation amplitude and φ is an arbitrary phase. In Fig. 13, we report a magnification of the bifurcation diagram in the neighborhood of the largest periodic window (around $A = 3.84$) inside the chaotic window. In Fig. 13a, we show the unperturbed case, in Fig. 13c the perturbed one. In Fig. 13b and d, we report the Lyapunov exponent. We note that the procedure maintains chaos in a large region of φ values, by narrowing the periodic window. Moreover, it is also able to control chaos: in fact we note a narrow periodic window around $A = 3.86$, not present in the unperturbed diagram. In our calculation we used

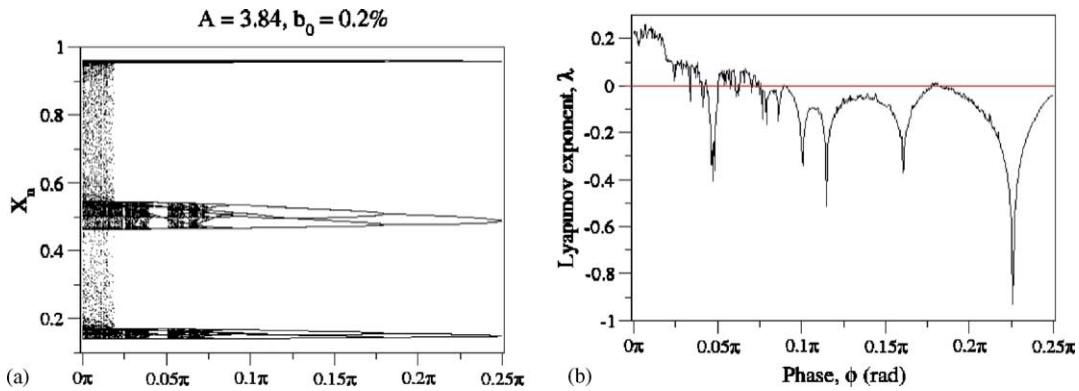

Fig. 14. (a) Bifurcation diagram x_n as a function of φ for the logistic map at $A = 3.84$ and (b) the related Lyapunov exponent. Not all φ values are effective in sustaining chaos: the phase must be properly chosen.

600 different values for A, with 1500 iterated for each A, recording the last 200 to avoid transients.

We also build a bifurcation diagram by fixing the modulation amplitude at $A_0 = 3.84$ and varying the phase. We have varied the phase from 0 to $\pi/4$ (for A values greater than $\pi/4$ the diagram repeats itself symmetrically with respect to $A = \pi/4$); this bifurcation diagram can be seen in Fig. 14. It is clear from this figure that there are some φ values for which the perturbation is effective, but there are some other one for which the behavior is again periodic. This result confirm the relevance of the relative phase term φ in the procedure. Because our method is effective also on the logistic map, the technique can be extended to discrete dynamical systems.

References

[1] T. Shimbrot, E. Ott, C. Grebogi, J.A. Yorke, Nature 363 (1993) 411;
S. Boccaletti, C. Grebogi, Y.-C. Lai, H. Mancini, D. Maza, Phys. Rep. 103 (2000).

[2] E. Ott, C. Grebogi, J.A. Yorke, Phys. Rev. Lett. 64 (1990) 1196;
W.L. Ditto, S.N. Rauseo, M.L. Spano, Phys. Rev. Lett. 65 (1990) 3211.

[3] I.B. Schwartz, I. Triandaf, Phys. Rev. Lett. 77 (1996) 4740.

[4] W. Yang, M. Ding, A.J. Mandell, E. Ott, Phys. Rev. E 51 (1995) 102.

[5] B. Peng, V. Petrov, K. Showalter, J. Phys. Chem. 95 (1991) 4957.

[6] P. Parmananda, P. Sherard, R.W. Rollins, H.D. Dewald, Phys. Rev. Lett. E 47 (1993) R3003.

[7] E.R. Hunt, Phys. Rev. Lett. 67 (1991) 1953;
R. Roy, T.W. Murphy, T.D. Maier, Z. Gills, E.R. Hunt, Phys. Rev. Lett. 68 (1992) 1259;
T.L. Carrol, I. Triandaf, I.B. Schwartz, L. Pecora, Phys. Rev. A 46 (1992) 6189;
Z. Gills, C. Iwata, R. Roy, I.B. Schwartz, I. Triandaf, Phys. Rev. Lett. 69 (1992) 3169.

[8] K. Pyragas, Phys. Lett. A 170 (1992) 421;
K. Pyragas, A. Tamaševicius, Phys. Lett. A 180 (1993) 99;
S. Bielawski, D. Derozier, P. Glorieux, Phys. Rev. E 50 (1994) 245;
S. Boccaletti, F.T. Arecchi, Europhys. Lett. 31 (1995) 127;
R. Meucci, M. Ciofini, R. Abbate, Phys. Rev. E 53 (1996) R5537;
S. Boccaletti, D. Maza, H. Mancini, R. Genesio, F.T. Arecchi, Phys. Rev. Lett. 79 (1997) 5246;
D.W. Sukow, M.E. Bleich, D.J. Gauthier, J.E.S. Socolar, Chaos 7 (1997) 560.

[9] R. Lima, M. Pettini, Phys. Rev A 41 (1990) 726.

[10] L. Fronzoni, M. Giocondo, M. Pettini, Phys. Rev. A 43 (1991) 6483.

[11] Y. Braiman, I. Goldhirsch, Phys. Rev. Lett. 66 (1991) 2545.

[12] A. Azevedo, S.M. Rezende, Phys. Rev. Lett. 66 (1991) 1342.

[13] R. Corbalan, J. Cortit, A.N. Pisarchik, V.N. Chizhevsky, R. Vilaseca, Phys. Rev. A 51 (1995) 663.

[14] J. Yang, Z. Qu, G. Hu, Phys. Rev. E 53 (1996) 4402.

[15] R. Chacón, J. Diaz Bejarano, Phys. Rev. Lett. 71 (1993) 3103;
R. Chacón, Phys. Rev. Lett. 86 (2001) 1737.

[16] D. Dangoisse, J.-C. Celet, P. Glorieux, Phys. Rev. E 56 (1997) 1396.

[17] V. In, et al., Chaos 7 (1997) 605.

[18] M. Dhamala, Y.-C. Lai, Phys. Rev. E 59 (1999) 1646.

[19] G.D. VanWiggeren, R. Roy, Science 279 (1998) 1198.

[20] I.T. Georgiou, I.B. Schwartz, SIAM J. Appl. Math. 59 (1999) 1178.

[21] I.B. Schwartz, I.T. Georgiou, Phys. Lett. A 242 (1998) 307.

[22] C. Grebogi, E. Ott, J.A. Yorke, Physica D 7 (1983) 181.

[23] K.T. Alligood, T.D. Sauer, J.A. Yorke, Chaos, Springer, New York, 1997.

[24] I.B. Schwartz, Phys. Rev. Lett. 60 (1988) 1359.

[25] V. In, S.E. Mahan, W.L. Ditto, M.L. Spano, Phys. Rev. Lett. 74 (1995) 4420.

[26] S. Codreanu, Chaos, Solitons Fractals 13 (2002) 839.

[27] V. In, M. Spano, M. Ding, Phys. Rev. Lett. 80 (1998) 700.

[28] I. Triandaf, I.B. Schwartz, Phys. Rev. E 62 (2000) 3529.

[29] K. Myneni, T.A. Barr, N.J. Corron, S.D. Pethel, Phys. Rev. Lett. 83 (1999) 2175.

[30] T.C. Newell, A. Gavrielides, V. Kovanis, D. Sukow, T. Erneux, S.A. Glasgow, Phys. Rev. E 56 (1997) 7223.

[31] R. Meucci, W. Gadomski, M. Ciofini, F.T. Arecchi, Phys. Rev. E 49 (1994) R2528.

[32] V.N. Chizhevsky, R. Corbalán, A.N. Pisarchik, Phys. Rev. E 56 (1997) 1580.

[33] I.B. Schwartz, I. Triandaf, R. Meucci, T.W. Carr, Phys. Rev. E 66 (2002) 026213.

[34] I. Triandaf, E. Bollt, I.B. Schwartz, Phys. Rev. E 67 (2003) 037201.